MODELING OF A HOLONOMIC OMNI-DIRECTIONAL VEHICLE WITH CONVENTIONAL TIRES

Lonnie J. Love
Robotics and Energetic Systems
Oak Ridge National Laboratory
Oak Ridge, TN 37831
lovelj@ornl.gov

John F. Jansen
Robotics and Energetic Systems
Oak Ridge National Laboratory
Oak Ridge, TN 37831
lovelj@ornl.gov

Abstract: In this paper, we explore the modeling and control of a holonomic omnidirectional vehicle using conventional wheels. We begin with a review of the basic approaches to omni-directional vehicle design based on holonomic wheel designs. While attractive from a controls perspective, these wheels are limited to low speed applications, can only operate on smooth surfaces, and require custom designed components. It is possible to design an omnidirectional vehicle using conventional wheel designs. This approach permits high payloads, high speeds, and operation on uneven ground. The penalty is added control complexity. This paper focuses on the modeling, control and simulation of an omnidirectional vehicle using conventional wheels. The primary contribution of this paper is the development of a basic methodology for computing the kinematics and dynamic equations of motion for a general holonomic omnidirectional vehicle using conventional wheels. This basic approach extends the work of Wada to include the ability to model nonlinear wheel friction, external body forces on the vehicle and internal body forces on the vehicle due to tracking errors on the wheels. We provide, as an example, a test case based on a 5000 lb vehicle with a 10,000 lb payload capacity that is presently being developed for the Navy.

1. Introduction

An omnidirectional platform provides the capability of independently translating and orienting itself without having first to reorient its wheels. Such platforms permit tight and efficient maneuvering in densely occupied environments. Commercial examples include an omnidirection wheelchair based on our Orthogonal Wheel concept and an omnidirectional forklift based on the Universal Wheel.[1,2] There are four major types of omnidirectional, holonomic wheeled systems: (1) the Universal Wheel (also known as Ilonator Wheels, or Mecanum Wheels, or Swedish Roller Wheels) which involves a set of rollers at the circumference of a hub;[3,4,5] (2) the Spherical Wheel [6,7]; (3) the Omni-Track, which utilizes ball wheels arranged in a crawler mechanism [8]; and (4) the Off-Centered In-Line Orientable Wheels (OCILOW) [9,10,11]. The first two designs benefit from the advantage of requiring only one motor per wheel (a minimum of three wheels) and very simple controls. However, they suffer from non-continuous rolling surfaces (with the point of contact changing from one roller to the next) that lead to significant vibrations when traversing over non-perfectly smooth terrain or when carrying high payloads. They also suffer from significant controls and stability problems at higher speeds. The third design involves a relatively large number of ball wheels which, on uneven terrain, alternate contact with the ground and suffer from differential friction during rotational motion and difficulty in handling heavy loads (multi-tons). The latter design, the OCILOW, requires two motors per wheel and more advanced controls because of the inter-wheel and intra-wheel constraints involved in the design. However it benefits from a continuous rolling surface on its conventional wheels, excellent high-speed behavior, and is ideal for high-payload conditions and uneven terrain (including potholes, ramps, steps and discontinuities, etc).[12]

The U.S. Navy is presently exploring advanced robotic and material handling technologies for their future carrier program. ORNL has explored the possibility of designing omnidirectional platforms for the Navy using both the Universal and Ball Wheel concepts (see Figure 1 through Figure 5). The Next Generation Munitions Handler (NGMH), developed by ORNL and showing in Figure 5, is a strength amplifying machine with an omnidirectional base using spherical wheels. While successful in demonstrating the technologies in the laboratory, the system experienced difficulty operating on uneven or rough terrain. Based on the very extensive experiments and studies performed at ORNL with high-payload wheeled platform designs to assess their suitability conditions, the only suitable concept is the OCILOW system, because it is capable of handling heavy loads (i.e., multi-ton), utilizing standard "off-the-shelf" wheels and tires that are suited for motions at high speed or on uneven terrain, while achieving true omnidirectional holonomic motion capabilities.

Figure 1: Universal Wheel

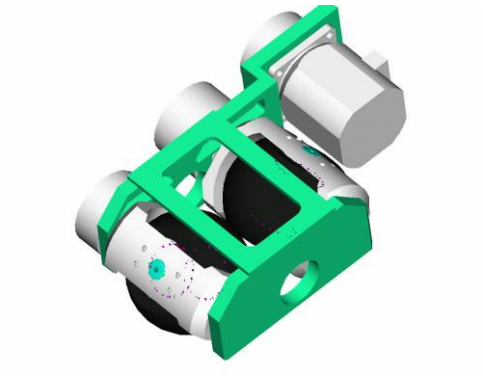

Figure 2: ORNL Holonomic Wheel

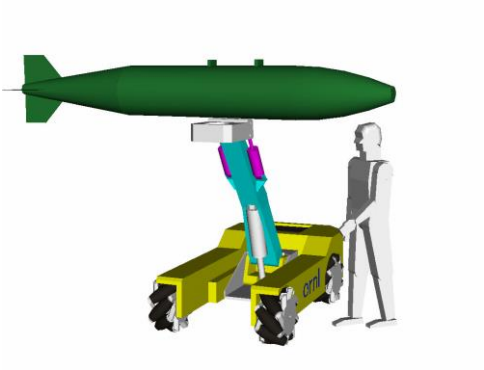

Figure 3: NGMH with Universal Wheel

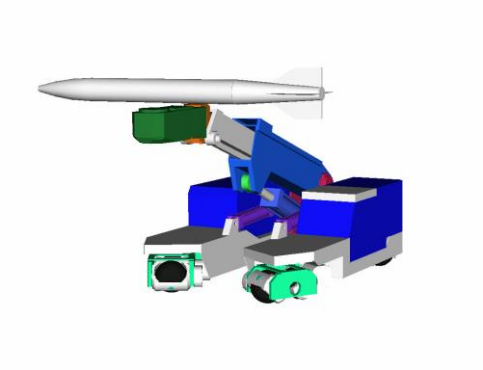

Figure 4: NGMH with ORNL Holonomic Wheels

Figure 5: ORNL's NGMH

The following manuscript begins with a background description of the Off-Center In-Line Orientable Wheels (OCILOW) in Section 2. The basic kinematics, transforming Cartesian velocity commands to steering and wheel velocity commands is covered in Section 3. In Section 4, we use Hamilton's principle to derive the dynamic equations of motion for a general OCILOW based omnidirectional vehicle, using any number of wheel pods. We extend the earlier work of Wada to include the computation of wheel interaction forces.[10] In addition, we construct a nonlinear model of the tire friction that includes variation in loading due to steering configuration as well as rolling and turning resistance. The motivation is to understand how the control of the steering and wheels impacts internal forces on the vehicle and wheel slippage. In Section 5, we use the resulting dynamic equations of motion to construct a Simulink model of a proposed omnidirectional vehicle we are presently designing for the Department of Navy. This system has four active wheel pods, a vehicle weight of 5000 lbs, a payload capacity of 10,000 lbs, and a top omnidirectional speed of 1 mph. The simulation serves as a preliminary analysis tool for the selection of actuation elements, power requirements, and sensing and control design.

2. Motivation for Inline Steering

We now explore the potential for using nonholonomic wheels for omnidirectional vehicles. An omnidirectional vehicle requires the ability, like the holonomic wheels described previously, that each wheel pod can immediately provide a velocity vector in any arbitrary direction. There are three fundamental approaches to conventional steering of wheels that we will briefly consider for use on an omnidirectional vehicle. The first configuration, Figure 6, has the steering axis set slightly to the side of the tire. With this configuration, both actuation of the steering and wheel motors provides an instantaneous velocity vector that is in line with the direction of the tire. It is not possible, through any combination of the steering and wheel motors to immediately provide a velocity vector on the vehicle in any arbitrary direction. The second approach, Figure 7, has the steering axis directly in line with the contact area between the wheel and tire. In the first configuration, there is a coupling between the steering action and the translation of the vehicle. By placing the steering axis in line with the contact area on the tire, this coupling is eliminated. However, it is still not possible to immediately impose an arbitrary velocity vector on the vehicle. Changing the direction requires first driving the steering axis then driving the wheel motor. There is only one approach, using conventional wheels, that provides the ability to impose an arbitrary velocity vector on the vehicle. This approach, shown in Figure 8, consists of placing the steering axis offset from the wheel contact axis, but in line with the wheel. Like the configuration in Figure 6, there is coupling between the wheel and steering motors. However, the primary difference is that the steering actuation provides a vector that is orthogonal to the velocity vector produced by the wheel actuator.

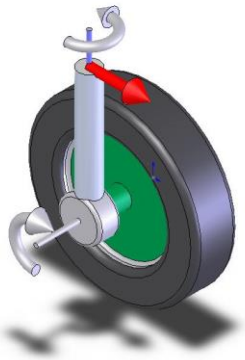

Figure 6: Offset Sideways Steered

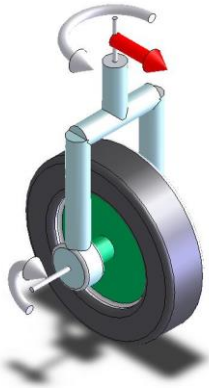

Figure 7: Inline Steered

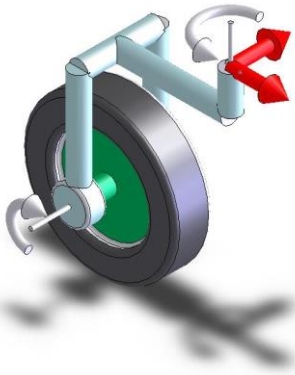

Figure 8: Offset Inline Steered

So, it is clearly possible to control a conventional wheel as if it were nonholonomic if the steering is configured properly. We will from this point forward refer to the wheel configuration in Figure 8 as Off-Center, In-Line, Orientable Wheels (OCILOW). Some of the advantages to this approach include high speed and high payload capacity and use of off-the-shelf components. However, the penalty is the complexity of the control.

3. Vehicle Kinematics

As stated early, the advantage to the omnidirectional wheel design is that there the control is very simple. Each wheel provides motion in one direction and is free to roll in the orthogonal direction. Any tracking error in the control of the individual wheel motors results only in tracking error of the overall vehicle. This is not the case for the OCILOW vehicle described above. Each wheel is constrained to move only in the rolling direction. Tracking error of each wheel results not only in loss of vehicle tracking, but also the buildup of internal forces in the vehicle frame (the wheels are fighting each other) or wheel slippage. Each wheel has two motors: a steering motor with velocity $\dot{\beta}$ and a wheel motor with velocity $\dot{\phi}$. Figure 4 shows the basic configuration for each wheel pod. Likewise, Figure 5 shows the basic notation we will use for a vehicle that has a total of four wheel pods. Equation (1) is the target vehicle velocity with respect to the vehicle's frame, X_vY_v.

$$\dot{\zeta} = \left[\dot{x}\ \dot{y}\ \dot{\theta}\right]^t \tag{1}$$

The objective of the kinematic analysis is to establish a closed form solution of the vehicle's steering and wheel velocities (Equations (2) and (3) respectively) as a function of the target vehicle velocity.

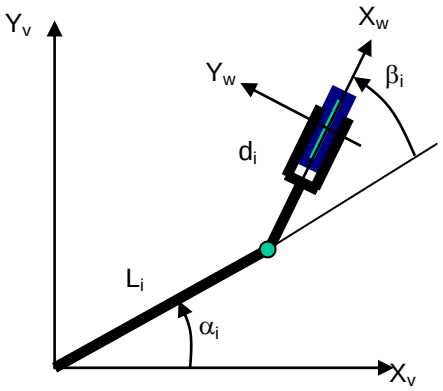

Figure 9: Wheel Pod Notation

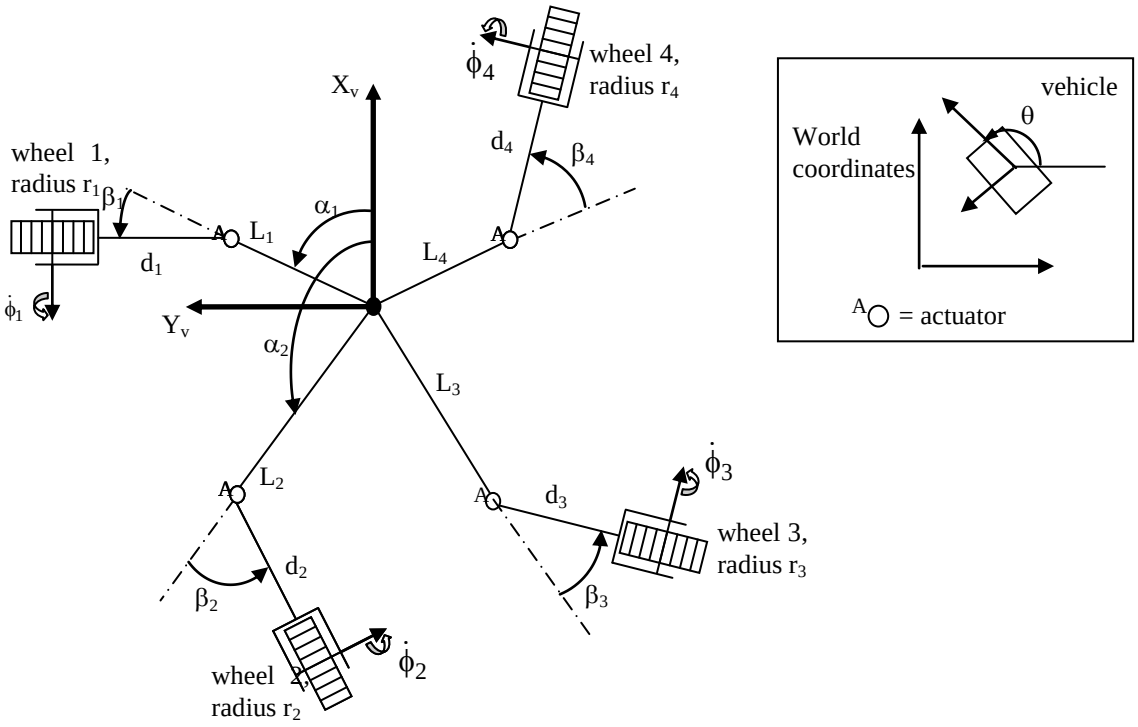

Figure 10: Vehicle Notation

$$\dot{\bar{\beta}} = \left[\dot{\beta}_1 \;\; \dot{\beta}_2 \ldots \dot{\beta}_M\right]^t \tag{2}$$

$$\dot{\bar{\phi}} = \left[\dot{\phi}_1 \;\; \dot{\phi}_2 \ldots \dot{\phi}_M\right]^t \tag{3}$$

Given a target vehicle velocity, $\dot{\zeta} \in \Re^3$, we can construct two constraints for each wheel pod, expressed in Equation (4). The constraints physically represent the no slip condition for the wheel.

$$\begin{aligned} &\left[\cos(\alpha_i+\beta_i+\theta) \;\; \sin(\alpha_i+\beta_i+\theta) \;\; L_i\sin(\beta_i)\right]\dot{\zeta} + r_i\dot{\phi}_i = 0 \quad \Rightarrow \; J_1^i\dot{\zeta} + J_2^i\dot{\phi}_i = 0 \\ &\left[-\sin(\alpha_i+\beta_i+\theta) \;\; \cos(\alpha_i+\beta_i+\theta) \;\; \left(L_i\sin(\beta_i)+d_i\right)\right]\dot{\zeta} + d_i\dot{\beta}_i = 0 \quad \Rightarrow \; C_1^i\dot{\zeta} + C_2^i\dot{\beta}_i = 0 \end{aligned} \tag{4}$$

We now combine all of the constraints for each wheel pod into a single expression, Equation (5), that couples the steering and wheel velocities of all of the pods to the target vehicle velocity. For a general vehicle with N wheel pods, the objective of the kinematic transformation in Equation (5) is to establish a closed form solution for the velocity vector, $\dot{q} \in \Re^{2N}$ which contains the wheel and steering velocity of each wheel pod, as a function of the Cartesian velocity vector. First note that the transformation $\Gamma \in \Re^{2Nx3}$ is a function of both θ and β and is easily computed. More importantly, the second transformation, $\Pi \in \Re^{2Nx2N}$ is not only diagonal, but the elements are the steering radius, d, and wheel radius r. So, it is clear that the transformation from a Cartesian velocity vector to the desired wheel and steering velocity vectors, Equation (6), is straightforward. It is clear that velocity control is quite possible for a vehicle with any number of active wheel pods. However, we need to now understand what occurs when tracking is not perfect. For this, we will now detail the computation of the dynamic equations of motion for an OCILOW vehicle.

$$\begin{bmatrix} J_1^1 \\ C_1^1 \\ \vdots \\ J_1^N \\ C_1^N \end{bmatrix}\dot{\zeta} + \begin{bmatrix} J_2^1 & 0 & \cdots & \cdots & 0 \\ 0 & C_2^1 & & & \\ \vdots & & \ddots & & \\ \vdots & & & J_2^N & \\ 0 & & & & C_2^N \end{bmatrix}\begin{Bmatrix} \dot{\phi}_1 \\ \dot{\beta}_1 \\ \vdots \\ \dot{\phi}_N \\ \dot{\beta}_N \end{Bmatrix} = \bar{0} \;\Rightarrow\; \Gamma\dot{\zeta} + \Pi\dot{q} = \bar{0} \tag{5}$$

$$\begin{Bmatrix} \dot{\phi}_1 \\ \dot{\beta}_1 \\ \vdots \\ \dot{\phi}_N \\ \dot{\beta}_N \end{Bmatrix} = \begin{bmatrix} J_2^1 & 0 & \cdots & \cdots & 0 \\ 0 & C_2^1 & & & \\ \vdots & & \ddots & & \\ \vdots & & & J_2^N & \\ 0 & & & & C_2^N \end{bmatrix}^{-1}\begin{bmatrix} J_1^1 \\ C_1^1 \\ \vdots \\ J_1^N \\ C_1^N \end{bmatrix}\dot{\zeta} \tag{6}$$

4. Vehicle Dynamics

When formulating the dynamics of the OCILOW vehicle, there are many issues to consider. First, the system is overconstrained. The vehicle configuration is $q \in \Re^{2N}$, but the motion is restricted to $\dot{\zeta} \in \Re^3$. Subsequently, there are 2N-3 constraints. In addition, we must include not only actuation forces, but external forces acting on the vehicle. To simplify the integration of kinematic constraints, external forces and the vehicle dynamics, we formulate the dynamic equations of motion using Hamilton's principle, Equation (7).

$$\int_{t_1}^{t_2}\left(\delta T+\delta\overline{W}\right)dt=0 \tag{7}$$

We begin with the formulation of the kinetic energy. There are five sources of mass: the vehicle body with mass M_v and rotary inertia I_v, each of the wheel pod's mass and inertia (M_p and I_β, respectively) and the wheel rotary inertia, I_ϕ. The only term that requires some additional attention is the kinetic energy due to the motion of the wheel pod's mass. Equation (8) provides the express for the wheel pod velocity with respect to a stationary frame from which $\dot{\zeta}$ is defined.

$$\begin{aligned} v_i &= \begin{Bmatrix} \dot{x}-L_i\dot{\theta}_i\sin(\alpha_i)-d_i\left(\dot{\theta}_i+\dot{\beta}_i\right)\sin(\alpha_i+\beta_i) \\ \dot{y}+L_i\dot{\theta}_i\cos(\alpha_i)+d_i\left(\dot{\theta}_i+\dot{\beta}_i\right)\cos(\alpha_i+\beta_i) \end{Bmatrix} \\ &= \begin{bmatrix} 1 & 0 & -L_i\sin(\alpha_i)-d_i\sin(\alpha_i+\beta_i) \\ 0 & 1 & L_i\cos(\alpha_i)+d_i\cos(\alpha_i+\beta_i) \end{bmatrix}\dot{\bar{\zeta}}+\begin{bmatrix} -d_i\sin(\alpha_i+\beta_i) \\ d_i\cos(\alpha_i+\beta_i) \end{bmatrix}\dot{\beta}_i \\ &= S_1(\beta_i)\dot{\bar{\zeta}}+S_2(\beta_i)\dot{\beta}_i \end{aligned} \tag{8}$$

Equation (9) provides the resulting kinetic energy of the vehicle.

$$\begin{aligned} T &= \frac{1}{2}\dot{\bar{\zeta}}^tM\dot{\bar{\zeta}}+\frac{1}{2}M_p\left(S_1(\beta)\dot{\bar{\zeta}}+S_2(\beta)\dot{\beta}\right)^t\left(S_1(\beta)\dot{\bar{\zeta}}+S_2(\beta)\dot{\beta}\right)+\frac{1}{2}\dot{\bar{\phi}}^tI_\phi\dot{\bar{\phi}}+\frac{1}{2}\dot{\bar{\beta}}^tI_\beta\dot{\bar{\beta}} \\ M &= \begin{bmatrix} M_v & 0 & 0 \\ 0 & M_v & 0 \\ 0 & 0 & I_v \end{bmatrix},\ I_\phi(i,j)=I_{\phi i}\delta(i,j),\ I_\beta(i,j)=I_{\beta i}\delta(i,j) \end{aligned} \tag{9}$$

We now formulate an expression for the work imposed on the system, Equation (10). The first represents the work due to an external force (force vector and torque), $F_v\in\Re^3$, acting on the vehicle. The second and third terms, $\tau_\beta\in\Re^N$ and $\tau_\phi\in\Re^N$, are the steering and wheel torque vectors respectively. The final two terms are the constraints on the system, defined previously. The Lagrange multipliers, $\lambda_\beta\in\Re^N$ and $\lambda_\phi\in\Re^N$, represent the internal forces on the wheel pods in the steering and wheel directions respectively. We will show shortly how these terms can be used not only to measure internal forces on the system, but also predict slippage.

$$W=\zeta^tF_v+\beta^t\tau_\beta+\phi^t\tau_\phi+\left(C_1(\beta)\dot{\bar{\zeta}}+C_2\dot{\bar{\beta}}\right)^t\bar{\lambda}_\beta+\left(J_1(\beta)\dot{\bar{\zeta}}+J_2\dot{\bar{\phi}}\right)^t\bar{\lambda}_\phi \tag{10}$$

We now define the variational of both the kinetic energy and work terms, Equations (11) and (12), respectively.

$$\begin{aligned} \delta T &= \delta\dot{\bar{\zeta}}^tM\dot{\bar{\zeta}}+\delta\dot{\bar{\phi}}^tI_\phi\dot{\bar{\phi}}+\delta\dot{\bar{\beta}}^tI_\beta\dot{\bar{\beta}}+ \\ &\quad M_p\left\{\delta\dot{\bar{\zeta}}^tS_1^t(\beta)S_1(\beta)\dot{\bar{\zeta}}+\delta\dot{\bar{\zeta}}^tS_1^t(\beta)S_2(\beta)\dot{\bar{\beta}}+\delta\dot{\bar{\beta}}^tS_2^t(\beta)S_1^t(\beta)\dot{\bar{\zeta}}+\delta\dot{\bar{\zeta}}^tS_2^t(\beta)S_2(\beta)\dot{\bar{\zeta}}\right\} \end{aligned} \tag{11}$$

$$\delta W=\delta\zeta^tF_v+\delta\beta^t\tau_\beta+\delta\phi^t\tau_\phi+\left(\delta\zeta^tC_1^t(\beta)+\delta\beta^tC_2^t\right)\bar{\lambda}_\beta+\left(\delta\zeta^tJ_1^t(\beta)+\delta\phi^tJ_2^t\right)\bar{\lambda}_\phi \tag{12}$$

When we combine the energy and work terms and substitute into Equation (7), we use integration by parts to eliminate the derivitive terms on the variationals, Equation (13).

$$\int_{t_1}^{t_2}\left(\delta T+\delta\overline{W}\right)dt=\int_{t_1}^{t_1}\left\{\begin{aligned} &\delta\zeta^tF_v+\delta\beta^t\tau_\beta+\delta\phi^t\tau_\phi+\left(\delta\zeta^tC_1^t(\beta)+\delta\beta^tC_2^t\right)\bar{\lambda}_\beta+\left(\delta\zeta^tJ_1^t(\beta)+\delta\phi^tJ_2^t\right)\bar{\lambda}_\phi-\delta\bar{\zeta}^tM\ddot{\bar{\zeta}}-\delta\bar{\phi}^tI_\phi\ddot{\bar{\phi}}-\delta\bar{\beta}^tI_\beta\ddot{\bar{\beta}}+ \\ &-M_p\left\{\delta\bar{\zeta}^tS_1^t(\beta)S_1(\beta)\ddot{\bar{\zeta}}+\delta\bar{\zeta}^tS_1^t(\beta)S_2(\beta)\ddot{\bar{\beta}}+\delta\bar{\beta}^tS_2^t(\beta)S_1^t(\beta)\ddot{\bar{\zeta}}+\delta\bar{\zeta}^tS_2^t(\beta)S_2(\beta)\ddot{\bar{\zeta}}\right\} \\ &-M_p\left\{\delta\bar{\zeta}^t\frac{\partial}{\partial t}\left(S_1^t(\beta)S_1(\beta)\right)\dot{\bar{\zeta}}+\delta\bar{\zeta}^t\frac{\partial}{\partial t}\left(S_1^t(\beta)S_2(\beta)\right)\dot{\bar{\beta}}+\delta\bar{\beta}^t\frac{\partial}{\partial t}\left(S_2^t(\beta)S_1^t(\beta)\right)\dot{\bar{\zeta}}+\delta\bar{\zeta}^t\frac{\partial}{\partial t}\left(S_2^t(\beta)S_2(\beta)\right)\dot{\bar{\zeta}}\right\} \end{aligned}\right\}dt \tag{13}$$

We now from Hamilton's principle that the expression inside the integral must be zero. Subsequently, we combine all like terms and are left with the final solution in Equation (14).

$$\begin{aligned}
&\delta\zeta^t\left\{F_v + C_1^t(\beta)\bar{\lambda}_\beta + J_1^t(\beta)\bar{\lambda}_\phi - \left(M + M_p S_1^t(\beta)S_1(\beta)\right)\ddot{\bar{\zeta}} - M_p S_1^t(\beta)S_2(\beta)\ddot{\bar{\beta}} - M_p\frac{\partial}{\partial t}\left(S_1^t(\beta)S_1(\beta)\right)\dot{\bar{\zeta}} - M_p\frac{\partial}{\partial t}\left(S_1^t(\beta)S_2(\beta)\right)\dot{\bar{\beta}}\right\} + \\
&\delta\beta^t\left\{\tau_\beta + C_2^t\bar{\lambda}_\beta - \left(I_\beta + M_p S_2^t(\beta)S_2(\beta)\right)\ddot{\bar{\beta}} - M_p S_2^t(\beta)S_1(\beta)\ddot{\bar{\zeta}} - M_p\frac{\partial}{\partial t}\left(S_2^t(\beta)S_2(\beta)\right)\dot{\bar{\beta}} - M_p\frac{\partial}{\partial t}\left(S_2^t(\beta)S_1(\beta)\right)\dot{\bar{\zeta}}\right\} + \\
&\delta\phi^t\left\{\tau_\phi + J_2^t\bar{\lambda}_\phi - I_\phi\ddot{\bar{\phi}}\right\} = 0
\end{aligned} \tag{14}$$

From calculus of variations, we know that all of the expressions coupled with the variational vectors must be zero as well providing the resulting equations of motion and constraints in Equations (15) through (19).

$$\begin{aligned}
&M_\zeta\ddot{\bar{\zeta}} + M_{\zeta\beta}\ddot{\bar{\beta}} + D_\zeta = F_v + C_1^t(\beta)\bar{\lambda}_\beta + J_1^t(\beta)\bar{\lambda}_\phi \\
&M_\zeta = \left(M + M_p S_1^t(\beta)S_1(\beta)\right),\ M_{\zeta\beta} = M_p S_1^t(\beta)S_2(\beta),\ D_\zeta = M_p\frac{\partial}{\partial t}\left(S_1^t(\beta)S_1(\beta)\right)\dot{\bar{\zeta}} + M_p\frac{\partial}{\partial t}\left(S_1^t(\beta)S_2(\beta)\right)\dot{\bar{\beta}}
\end{aligned} \tag{15}$$

$$\begin{aligned}
&M_\beta\ddot{\bar{\beta}} + M_{\zeta\beta}^t\ddot{\bar{\zeta}} + D_\beta = \tau_\beta + C_2^t\bar{\lambda}_\beta \\
&M_\zeta = \left(I_\beta + M_p S_2^t(\beta)S_2(\beta)\right),\ D_\zeta = \frac{\partial}{\partial t}\left(S_2^t(\beta)S_2(\beta)\right)\dot{\bar{\beta}} + M_p\frac{\partial}{\partial t}\left(S_2^t(\beta)S_1(\beta)\right)\dot{\bar{\zeta}}
\end{aligned} \tag{16}$$

$$I_\phi\ddot{\bar{\phi}} = \tau_\phi + J_2^t\bar{\lambda}_\phi \tag{17}$$

$$J_1(\beta)\dot{\zeta} + J_2\dot{\phi} = 0 \tag{18}$$

$$C_1(\beta)\dot{\zeta} + C_2\dot{\beta} = 0 \tag{19}$$

Finally, we need a way of combining these equation to solve for the motion and internal forces in the vehicle. One simple approach is shown in Equation (20). This basic format is easily integrated into a simulation environment such as Simulink. Each time step, the present inputs and states are used to compute the effective mass matrix and vector of combined inputs and nonlinear components (left side of Equation (20)). We then use a linear solver, such as Gauss elimination, to compute the acceleration terms and Lagrange multipliers.

$$\begin{bmatrix} M_\zeta & M_{\zeta\beta} & 0 & -J_1^t(\beta) & -C_1^t(\beta) \\ M_{\zeta\beta}^t & M_\beta & 0 & -J_2^t & 0 \\ 0 & 0 & M_\phi & 0 & -C_2^t \\ C_1(\beta) & C_2 & 0 & 0 & 0 \\ J_1(\beta) & 0 & J_2 & 0 & 0 \end{bmatrix}\begin{Bmatrix} \ddot{\zeta} \\ \ddot{\beta} \\ \ddot{\phi} \\ \lambda_\beta \\ \lambda_\phi \end{Bmatrix} = \begin{Bmatrix} F_v - D_\zeta \\ \tau_\beta - D_\beta \\ \tau_\phi \\ -\dot{C}_1(\beta)\dot{\zeta} \\ -\dot{J}_1(\beta)\dot{\zeta} \end{Bmatrix} \tag{20}$$

4.1. Tire Rolling and Turning Resistance

One last element of concern is the nonlinear friction associated with the tires. At low speeds on hard surfaces, the primary source of rolling resistance is caused by the hysteresis in the tire materials due to the defection of the materials while rolling. [13] As the tire deforms, a percentage of the strain energy is lost during recovery due to the hysteresis in the materials. In this study, we are focusing on low speed, high payload platforms. The tire materials we are using are a Kasalon Polyurethane, KAS67591AG which has an elastic modulus of 9200 psi, hysteresis of 9.2% and a static friction coefficient of 0.57. At low speeds we can assume a relatively uniform tire deformation,

shown in Figure 11. In reality, there are slight bulges in the materials in front of and behind the tire, but we neglect this for now to simplify the analysis.

First, we must know the load (F_{li}) on each wheel. We start by assuming the vehicle weight, mg, has a center of gravity (x_c,y_c) defined with respect to the frame X_vY_v in Figure 10. We know that for static equilibrium, the sum of forces in the vertical direction are zero and the sum of moments about the X_v and Y_v axes are zero. Equation (21) provides the resulting constraints for static equilibrium. Clearly, the system is statically indeterminant. We exploit the pseudo-inverse for a least squares estimate of the resulting wheel loads as a function of vehicle configuration.

$$\begin{bmatrix} 1 & 1 & 1 & 1 \\ L_1\cos(\alpha_1)+d_1\cos(\alpha_1+\beta_1) & L_2\cos(\alpha_2)+d_2\cos(\alpha_2+\beta_2) & L_3\cos(\alpha_3)+d_3\cos(\alpha_3+\beta_3) & L_4\cos(\alpha_4)+d_4\cos(\alpha_4+\beta_4) \\ L_1\sin(\alpha_1)+d_1\sin(\alpha_1+\beta_1) & L_2\sin(\alpha_2)+d_2\sin(\alpha_2+\beta_2) & L_3\sin(\alpha_1)+d_3\sin(\alpha_3+\beta_3) & L_4\sin(\alpha_4)+d_4\sin(\alpha_4+\beta_4) \end{bmatrix} \begin{Bmatrix} F_{l1} \\ F_{l2} \\ F_{l3} \\ F_{l4} \end{Bmatrix} = \begin{Bmatrix} mg \\ mgx_c \\ mgy_c \end{Bmatrix} \quad \textbf{(21)}$$

Given the wheel loads, we are ready to analyze the rolling resistance in the tires. We begin with a simplified model of the wheel deformation, Figure 11.

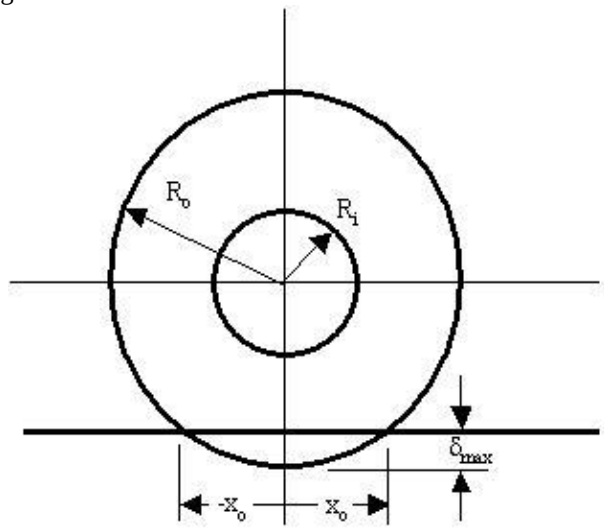

Figure 11: Wheel Model

The basic boundary conditions are that the deflection, δ, is zero at both x_0 and $-x_0$. Likewise, the tire deformation at the center of the wheel/ground contact area is δ_{max}. We use a simple cosine function to represent the tire deformation.

$$\delta(x) = \delta_{max}\cos\left(\frac{x}{x_0}\frac{\pi}{2}\right) \quad \textbf{(22)}$$

We assume an equilibrium condition where the potential energy of the loaded wheel is balanced by the strain energy in the tire (w is the tire width).

$$mg\delta_{max} = \int_{-x_0}^{x_0} \frac{Ew}{R_o - R_i}\left(\delta_{max}\cos\left(\frac{x}{x_0}\frac{\pi}{2}\right)\right)^2 dx \quad \textbf{(23)}$$

We evaluate the above equation and find a solution for the maximum deflection, $\delta_{max.}$

$$\delta_{max} = \left(\frac{F_l(R_o - R_i)}{Ew\sqrt{2R_o}}\right)^{2/3} \quad \textbf{(24)}$$

Formulation of the rolling resistance is based on computing the product of the material's hysteresis with the energy of deformation. We derive the deformation of materials as a function of an incremental rolling displacement of the wheel. This rotary displacement produces a material deformation in the elastic tire. There is a resulting strain energy due to this deformation. The rolling resistance is based on the product of the material's hysteresis with the strain energy (e.g. the hysteresis defines how much energy is lost due to deformation and expansion of the material).

The potential energy lost due to the compliance of the loaded wheel is $mg\delta_{max}$. The tire rolls (assuming small angles) approximately $\theta=2x_0/R_o$ radians for a full cycle of the material, shown in Figure 11 to fully compress and recover. The energy input into the tire is $\tau_r\theta$ while the energy lost is $h(mg)\ \delta_{max}$. Manipulation of this expression resulting in the rolling resistance, Equation (25), which closely matches the rolling resistance models provided by Kastalon (their product is 0.51 while the product from the above computation is 0.63). Also note that the load, mg, is the actual load on the tire, not the total vehicle weight.

$$\tau_r = \sqrt{1/2}\sqrt[3]{1/\sqrt{2}}\ h\sqrt[3]{\frac{F_l^4 R_o\left(R_o - R_i\right)}{Ew}} \tag{25}$$

In addition to the rolling resistance, there is a resistance due to turning. We formulate this term based on computing the strain energy due to the shearing action between the wheel and the road as the wheel is both turning and rolling. Figure 12 shows a simple model of the turning deformation of the tire. As the wheel is rotating and turning, there is a required angular deformation of the tire, δ_t. We can approximate this angle using Equation (26). It is clear that this deformation angle diverges as ω approaches zero. At this point, the material transitions from deforming to slipping.

$$\delta_t \cong \frac{\dot{\beta} x_o}{\omega R_o} \tag{26}$$

One approach to modeling the turning resistance is to estimate the shear stress required to deform the tire by the angle δ_t. The shear stress for an incremental surface element in the material is a function of the modulus of elasticity and poisson's ratio, υ. We can evaluate the turning resistance by integrating the shear stress over the entire contact surface area, Equation (27).

$$\tau_{turn\_hist} = \int_{-x_0}^{x_0}\int_{-w/2}^{w/2}\left(G\delta_t\sqrt{x^2+y^2}\right)dx\,dy \quad \text{where } G = \frac{E}{2(1+\upsilon)} \tag{27}$$

The evaluation of the double integral in Equation **(27)** proves to be quite complex. We simplify the model by assuming the shear stress is constant across the tread width.

$$\tau_{turn\_hist} = \int_{-x_0}^{x_0}\int_{-w/2}^{w/2}\left(G\delta_t\sqrt{x^2+y^2}\right)dx\,dy \Rightarrow \int_{-x0}^{x0} wG\delta_t x\,dx = wG\delta_t x_0^2 \tag{28}$$

As stated earlier, the term δ_t diverges as the wheel velocity approaches zero. There is a point in which the wheel turning resistance transitions from a shear stress model (Equation (28)) to sliding friction model. At this point, the shear stress between the tire and ground is a function of the product of the normal load and coefficient of friction, μ.

$$\tau_{turn\_fric} = 2\int_{0}^{x_0}\int_{-w/2}^{w/2}\mu\left(\frac{Ew}{R_o - R_i}\delta_{max}\cos\left(\frac{x}{x_0}\frac{\pi}{2}\right)\right)\sqrt{x^2+y^2}\,dx\,dy \tag{29}$$

We use the same argument as before for reducing the double integral to a simpler expression.

$$\begin{aligned}\tau_{turn\_fric} &\cong 2w\int_{0}^{x_0}\mu\left(\frac{Ewx}{R_o - R_i}\delta_{max}\cos\left(\frac{x}{x_0}\frac{\pi}{2}\right)\right)dx \\ &= 2w\mu\left(\frac{Ew}{R_o - R_i}\delta_{max}\frac{2}{\pi}\left(1-\frac{2}{\pi}\right)\right)x_o^2\end{aligned} \tag{30}$$

The model for the turning friction involves the solution for both models and using the smaller of the two solutions. The physical justification for this approach is that if the shear stress exceeds the sliding friction, the tire is in a sliding condition. An example of the rolling and turning resistance is displayed in Figure 16.

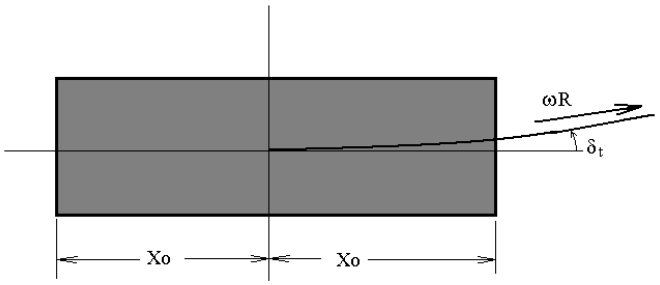

Figure 12: Turning Deformation

5. Simulation

Finally, we integrate all of the previous work in modeling into a numerical simulation. The simulink model used in this investigation is shown in Figure 13. The system has four active wheel pods, each of which are controlled by large electric motors. The motivation for such a detailed model is the ability to assist in sizing actuators, investigate control algorithms and estimate performance. Figure 14 displays a target trajectory that exercises the omnidirectionality of the vehicle. The system is commanded to first move in the y-direction, followed by an immediate translation in the x-direction. This is followed by a pure rotation and then a combined translation and rotation. Figure 15 displays the variation on the wheel loading as a function of the vehicle configuration. The rolling and turning resistance, shown in Figure 16, is calculated based on the models described previously. The resulting tracking response is displayed in various forms in Figure 17, Figure 18, and Figure 19. We compare the wheel/ground interaction force, based on the Lagrange multipliers, with the wheel traction to determine if the system ever reaches a slipping condition, see Figure 20. Finally, Figure 21 and Figure 22 display the wheel and turning torques during this maneuver.

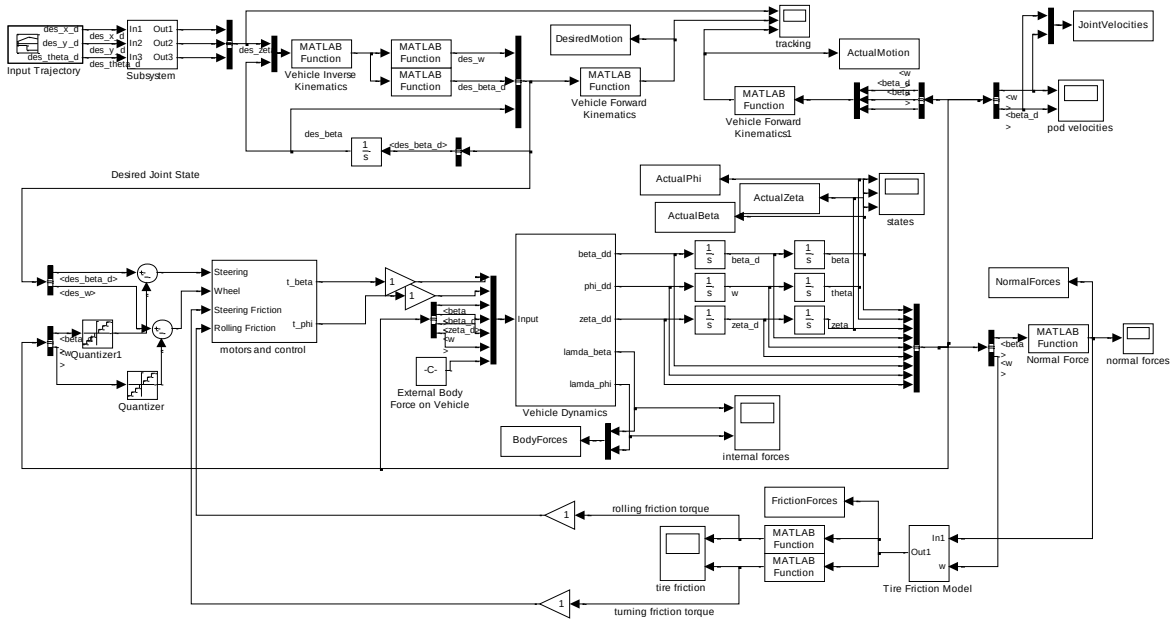

Figure 13: Simulink Model of OCILOW Vehicle

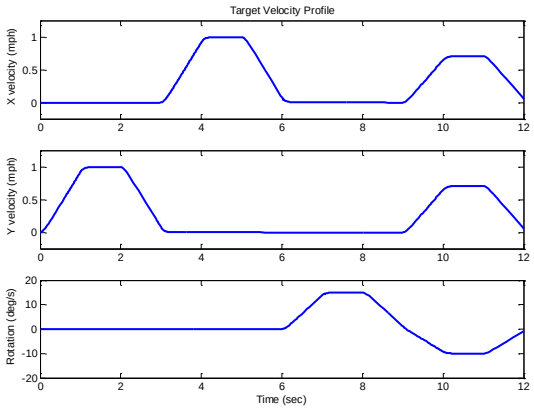

Figure 14: Target Trajectory

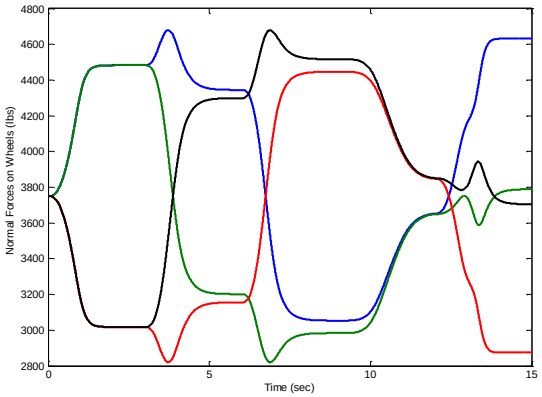

Figure 15: Normal Load on Wheels

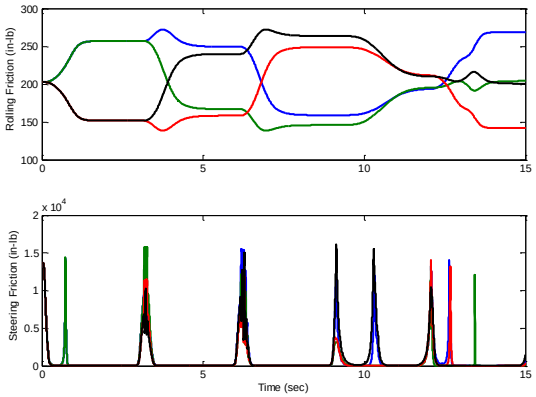

Figure 16: Rolling and Turning Resistance

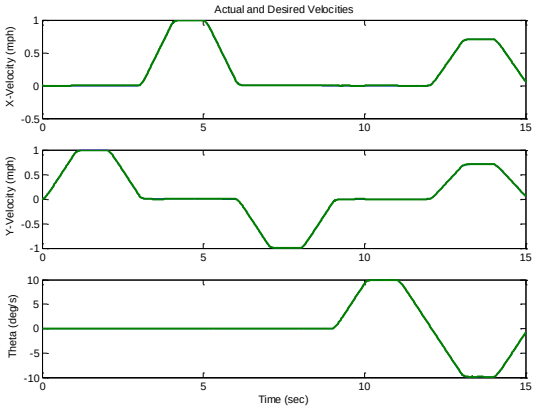

Figure 17: Time Response

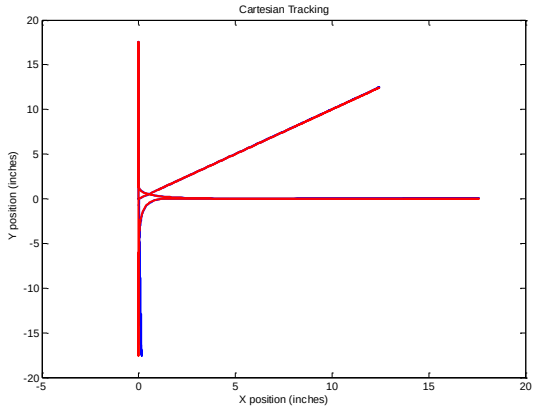

Figure 18: Spatial Response

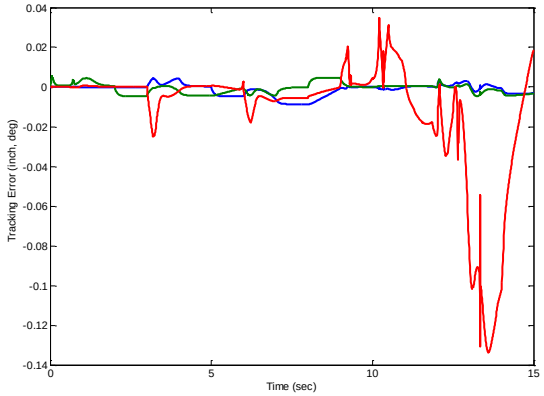

Figure 19: Tracking Error

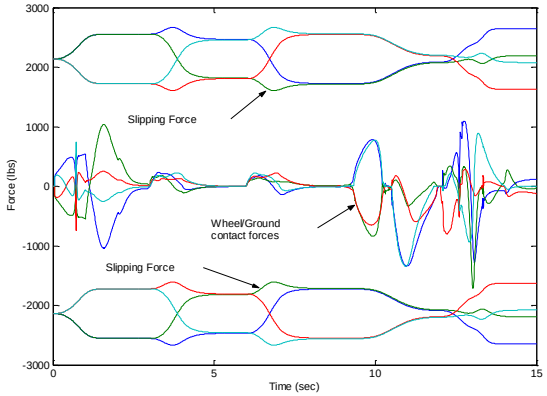

Figure 20: Traction

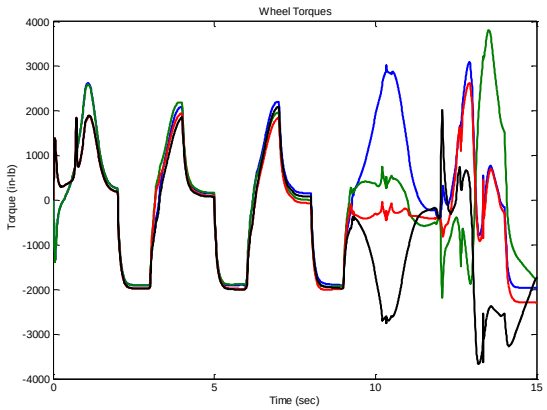

Figure 21: Wheel Torques

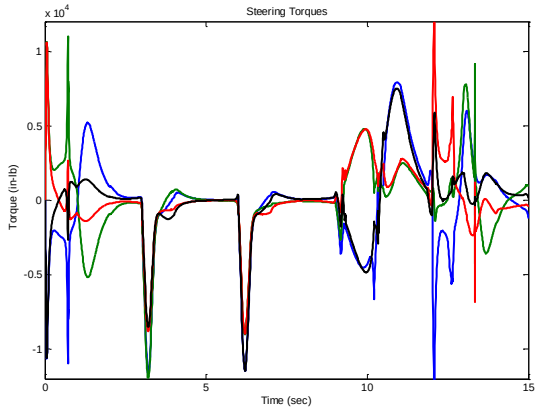

Figure 22: Turning Torques

Conclusions

This paper provides the fundamental motivation for developing omnidirectional vehicles based on conventional wheel designs. Omnidirectional wheels have the advantage of using a single actuator per wheel pod, compared to two actuators per wheel pod when using conventional wheels. In addition, the control of the vehicle is relatively straightforward. However, omnidirectional wheels are generally characterized as having difficulties when operating on uneven surfaces or higher speeds. Omnidirectional vehicles based on conventional wheel designs, while more complex in control, add the flexibility of having off-the-shelf components, operation on uneven surfaces, and the ability to transition to high-speed operations. We have extended the previous work in modeling omnidirectional vehicles to include external force inputs to the system and estimation of internal forces on the vehicle due to tracking errors. In addition, we have developed nonlinear rolling and turning resistance models for the wheels. The motivation for this work was to aid in the design and control of a future naval omnidirectional vehicle based on the off-center orientable wheels.

References

[1] http://www.oakridger.com/stories/052997/rover.html
[2] http://www.airtrax.com/default1.htm
[3] Ilon, B., "Wheels for a Course Stable Selfpropelling Vehicle Movable in any Desired Directon on the Ground or Some Other Base," U.S. Patent No. 3,876,255, 1975.

[4] Ferriere, L, Raucent, B., and Campion, G., "Design of Omnimobile Robot Wheels," *IEEE Conf. on Robotics and Automation*, 1996, pp. 3664-3670.
[5] Dickerson, S., and Lapin, B., "Control of an Omnidirectional Robotic Vehicle with Mecanum Wheels, Proceedings of Telesystems Conference, Vol.1., pp. 323-328, Mar 1991.
[6] Pin, F. G. and S. M. Killough, "A New Family of Omnidirectional and Holonomic Wheeled Platforms for Mobile Robots," *IEEE Transactions on Robotics and Automation* **10**(4), 480–489 (1994).
[7] West, M., and Asada, H., "Design of a Ball Wheel Mechanism for Omnidirectional Vehicles with Full Mobility and Invariant Kinematics," *Journal of Mechanical Design*, Vol. 119, pp. 153-161.
[8] West, M., and H. Asada, "Design of a Holonomic Omnidirectional Vehicle," *IEEE Conf. on Robotics and Automation*, May 1992, pp. 97-103.
[9] Campion, G., G. Bastin, B. D. Andrea-Novel, "Structural Properties and Classification of Kinematic and Dynamic Models of Wheeled Mobile Robots," *IEEE Conf. on Robotics and Automation*, May 1993, pp. 462-469.
[10] Wada, M., and Mori, S., "Holonomic and Omnidirectional Vehicles with Conventional Tires," *IEEE Conf. on Robotics and Automation*, 1996, pp. 3671-3676.
[11] Jung, M., and Kim, J., "Mobility Augmentation of Conventional Wheeled Bases for Omnidirectional Motion," IEEE Transactions on Robotics and Automation, Vol. 18, No. 1, pp. 81-87, 2002.
[12] Spenko, M., Yu, H., Dubowsky, S., "Analysis and Design of an Omnidirectional Platform for Operation on Non-Ideal Floors," *IEEE International Conference on Robotics and Automation*, Washington D.C, May 11-May 15 2002.
[13] Wong, J., Theory of Ground Vehicles, John Wiley and Sons, pp. 8-16, 1993.